2-D primary beam shape measurements of the band-3, 250–500 MHz of the uGMRT

Santaji N. Katore and Dharam V. Lal
snk/dharam AT ncra DOT tifr DOT res DOT in

September 12, 2023

Contents

List of Figures

List of Tables

Abstract

In interferometric images, knowledge of the primary beam is important in measurements of the flux densities and spectra of sources away from the pointing centre. Correction for the effect of the varying primary beam sensitivity is thus important in high dynamic imaging. Here, in this report, we present first measurements of the frequency dependent primary beam shapes for the band-3 (250–500 MHz) of the upgraded GMRT. These measurements would form a useful input for all users of the uGMRT.

1 Introduction

The recently accomplished upgrade of the GMRT (Gupta et al. 2017) has resulted in a significant increase in the instantaneous bandwidth of the telescope. This, it turn, leads to a significant increase in the sensitivity for continuum as well as pulsar studies. As part of the upgrade, all the antenna feeds, except the L-band feed have been replaced. Earlier measurements of the primary beam shape at Band-3 however were available only in the form of the best fit polynomial to an assumed azimuthally symmetric beam. Here we provide measurements of the actual 2-D shape of the beam in each polarization, which is significantly azimuthally asymmetric, as well as different for the two polarizations. However, for applications in which it is sufficient to assume an azimuthally symmetric polarization independent beam, we also provide polynomial fits to the same.

Note that the band-3 (250–500 MHz) feeds at the uGMRT are circularly polarized and they have been called as "RR", "LL" and hence, the stokes I is labeled as "RRLL" at the GMRT. In this report, here we continue using this labeling. Here we use these basics (see also 2-D primary beam shape measurements of the band-5, 1050–1450 MHz of uGMRT, S.N. Katore & J.N. Chengalur, for more details) and present the methodology in Section 2, data analysis in Section 3, and summarize our findings in Section 5.

2 Methodology and data acquisition

The observations were made in the interferometric mode, using observations of 3C sources (3C286, 3C48 and 3C147). The default frequency setup for continuum band-3, 250–500 MHz band observations was used for all observations.

- Bandwidth = 200 MHz,
- No. of channel = 2048,
- Frequency Range = from 300 MHz to 500 MHz, and
- GAB LO = 500 MHz.

The antennas were scanned in the azimuth axis, with the multiple scans spaced $11'$ apart along the elevation axis. The scan rate was $60'$/minute and the integration time was either 2 second or 4 second. The grid size was selected to cover the beam at least up to the first null.

Note that for high dynamic range imaging applications one would need to determine the primary beam to still farther distances than what our measurements provide. One would also need to know the full polar properties of the beam. As such, our measurements should be regarded only as a first step in the direction of characterizing the primary beam. We also note that the current feed positioning system at the GMRT has limited accuracy. This results in different primary beam shapes every time a feed is brought to focus. As such, it may in any case be difficult to apply the high dynamic range imaging techniques that use information about the primary beam. The current measurements may hence be adequate until the feed position system is upgraded.

3 Data analysis

A total of six data were obtained, three data sets on 24 December 2017, and one data set each on 9, 21 and 23 February 2019. After flagging out non functional antennas, the visibilities were used to determine antenna based gains, which was squared to get the power. The known raster scan rate and elevation position were used to convert the time-stamp of the data into the position on in the grid. The solution was computed independently for $\sim$0.097 MHz wide channels that are spaced $\sim$5 MHz apart to cover the frequency range from 300 MHz to 500 MHz. GNUPLOT was used to interpolate the observations onto a

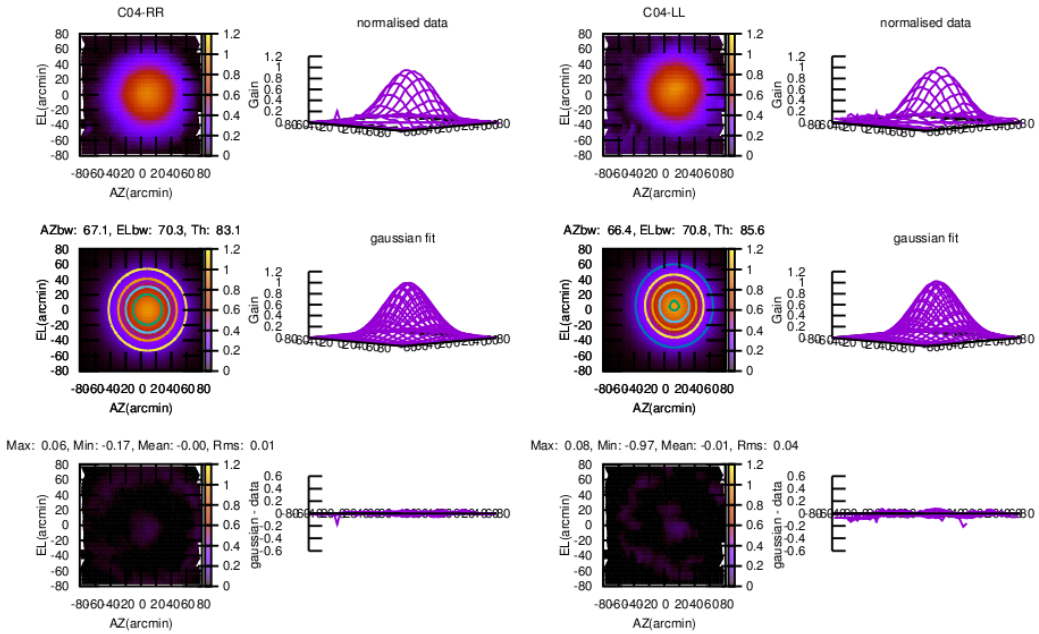

Figure 1: The data (top-panel) and the Gaussian fits (middle-panel) for the representative C 04 antenna at the centre frequency, 420 MHz of the band-3 (300–500 MHz) for the RR (left-column) and LL (right-column) polarizations. The bottom panel shows the difference between the data and the Gaussian fits showing the residuals.

uniform grid in altitude and azimuth for each polarization. A 2-D elliptical Gaussian was fit to each data set using GNUPLOT to parametrize the beam shape. This parametrization is used to study the variation of the beam with frequency and polarization. Specifically the 2-D beam data grid was parametrized using a function of the form:

$$f(x,y) = A \times e^{-(a(x-x_0)^2+2b(x-x_0)(y-y_0)+c(y-y_0)^2)} \tag{1}$$

where,

$$a = \frac{cos^2\theta}{2\sigma_x^2} + \frac{sin^2\theta}{2\sigma_y^2},$$

$$b = \frac{sin2\theta}{4\sigma_x^2} + \frac{cos2\theta}{4\sigma_y^2},$$

and

$$c = \frac{sin^2\theta}{2\sigma_x^2} + \frac{cos^2\theta}{2\sigma_y^2}.$$

Here the coefficient A is the amplitude, x_0, y_0 are the offsets from the center and σ_x, σ_y are the x and y spreads of the beam (major and minor axis), from which the "half power beam width" (HPBW) or "full width at half maximum" can be computed. The angle θ indicates the position angle, in case of an elliptical beam. Where the HPBW are

$$\mathrm{HPBW} = 2.35482 \times \sigma_x$$

and

$$\mathrm{HPBW} = 2.35482 \times \sigma_y$$

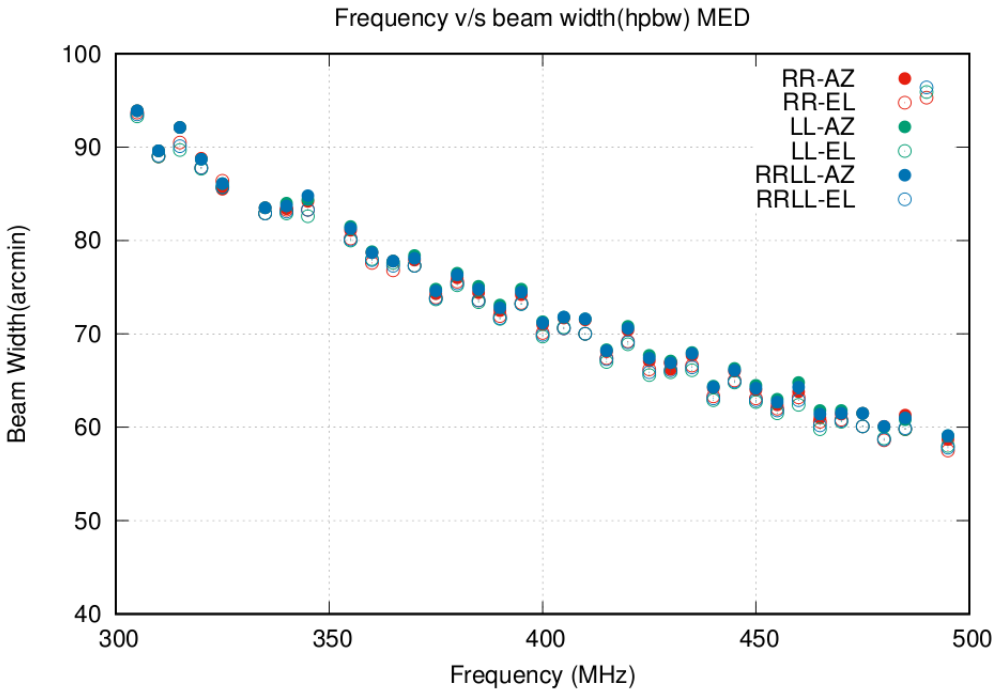

Figure 2: The plot showing the HPBW measured from the median of the six observing runs (for the data of all good antennas at each epochs) as a function of frequency. The three different colored points indicates the RR (shown in red), LL (shown in green) and RRLL (shown in blue). Recall that the RRLL label indicates stokes I. The solid-filled circles and empty circles are for the azimuth (AZ) and elevation (EL) axes, respectively. Missing points, if any, are due to the removal of RFI affected data.

for the major and minor axes, respectively. Furthermore, each Gaussian function is normalized to unity at the peak and the peak position was set to (0,0), i.e. the origin. To illustrate this, Fig. 1 shows the Gaussian fits for the C 04 antenna at the centre frequency, 420 MHz of the band-3 (250–500 MHz) for the RR and LL polarizations.

The gridded data for all good antennas were averaged together (pixel by pixel) to increase signal to noise and a single average data set was formed. This was done separately for the RR and LL polarizations at each frequency channel for each epoch. In addition a stokes I beam (labeled as "RRLL" in the Figures below) was generated by further averaging the data for the two polarization, RR and LL at each frequency channel for each epoch.

As stated above, a total of six observing runs were performed spread over a period between 24 December 2017 (three data sets) and one data set each on 9, 21 and 23 February 2019. After averaging the data sets, as described above for each epoch, we also computed a combined average (labeled as "AVG" in the Figures below) and a combined median (labeled as "MED" in the Figures below) data for all the six observing runs. We thus have azimuth and elevation beams for (i) RR polarisation, for (ii) LL polarization, and for (iii) RRLL (= Stokes I), all frequency-channels (spaced 5 MHz apart) of the 300–500 MHz band.

4 Systematic trends in the measurements

Below we discuss beam ellipticity, i.e., dependence of beam-width on the frequency. We use the polynomial fits for an azimuthally symmetric beam profile, and the accuracy of these polynomial fits in order

Table 1: The polynomial coefficients for the three polynomial fits of 8th order, 10th order and 12th order, respectively for the median (MED) RRLL beams. See also Sec. 4.3 and Fig. 6. Also detailed are the RMS', "data minus model" values for the 200% surface fit to should comparisons between these three polynomial fits.

Order	Polynomial coefficients					
	a	b	c	d	e	f
8th	−3.1290691	38.8158156	−21.6079225	4.4833790		
10th	−3.2547104	46.7394813	−37.6108878	17.3300744	−3.5526055	
12th	−3.3811418	58.0502647	−71.6977548	62.8117580	−31.2102179	6.2510507
	RMS values, "data minus model" for the 200% (HPBW) surface fit.					
8th		0.0159				
10th		0.0146				
12th		0.0140				

to understand systematic trends, if any in band-3, 250–500 MHz band data of the uGMRT.

4.1 Beam ellipticity

Fig. 2 shows the plot of the HPBW measured from the median of the six observing runs, for the data of all good antennas at each epochs, as a function of frequency. The three different colored points indicates the RR (shown in red), LL (shown in green) and RRLL (shown in blue). Recall that the RRLL label indicates stokes I. The solid / filled circles are for the azimuth (AZ) axis while the empty circles are for the elevation (EL) axis. Missing data, if any for a frequency in the Fig. 2 and subsequent Figures below are due to flagging, which is largely due to the removal of the RFI affected data.

As can be seen in Fig. 2, the RR and LL beams are elliptical, with the ellipticity being more pronounced at the lower frequencies. The major axis of the two ellipses are also misaligned, with one beam being wider along the elevation axis and the other beam being wider along the azimuth axis. Whereas the stokes I ("RRLL") beam has widths that is equal along the elevation and azimuth axes.

4.2 Scaling with frequency

Naively one would expect the beam width to scale linearly with wavelength. However, since the feed illumination may vary in a non trivial manner with wavelength, deviations from this simple scaling are possible. We hence did fits of both first and second order polynomials to the HPBW as a function of frequency, *viz.*,

$$f(x) = \frac{\lambda}{a_1}$$

is the first order polynomial, and

$$f(x) = \frac{\lambda}{a_1} + \frac{\lambda^2}{a_2}$$

is the second order polynomial. Where λ is wavelength, a_1 and a_2 are respectively the coefficients of the first and second order polynomials. The left-panel of Fig. 3 shows the first order polynomial fit to the beam width (RRLL) and the right panel shows the second order fit to the same beam width (RRLL). The lower two panels show the difference between the data and the model-fit for the first order polynomial fit (lower left-panel) and for the second order polynomial fit (lower right-panel). The fit to the data suggests that the second order polynomial fit is relatively better than the first order polynomial fit.

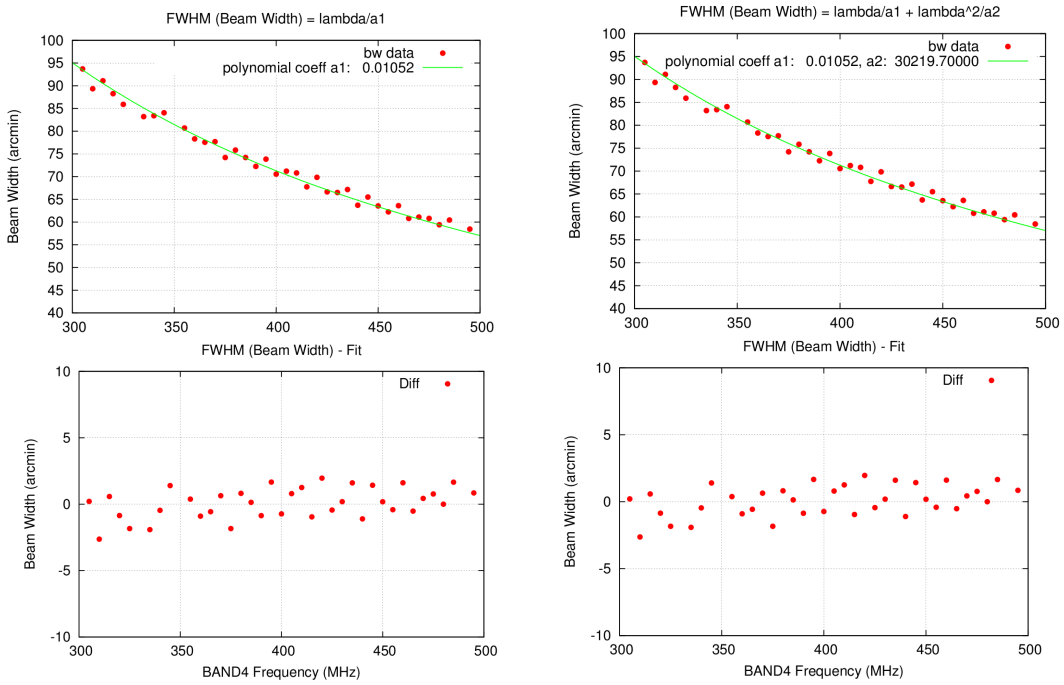

Figure 3: The upper left-panel shows the first order polynomial fit to the beam width (RRLL) data and the upper right-panel shows the second order polynomial fit to the same beam width (RRLL) data. The lower two panels show the difference between the data and the model-fit for the first order polynomial fit (lower left-panel) and second order polynomial fit (lower right-panel).

4.3 Azimuthally symmetric polynomial fits

As discussed above, the stokes I beam ("RRLL") can be reasonably well approximated to be azimuthally symmetric. We provide below 8th, 10th and 12th order polynomial fits to the beam for a user to infer, which of these three approximations is reasonably good.
The 8th order polynomial function is expressed as

$$f(x,y) = 1 + \frac{a}{10^3}(r\nu)^2 + \frac{b}{10^7}(r\nu)^4 + \frac{c}{10^{10}}(r\nu)^6 + \frac{d}{10^{13}}(r\nu)^8 \quad (2)$$

The 10th order polynomial function is expressed as

$$f(x,y) = 1 + \frac{a}{10^3}(r\nu)^2 + \frac{b}{10^7}(r\nu)^4 + \frac{c}{10^{10}}(r\nu)^6 + \frac{d}{10^{13}}(r\nu)^8 + \frac{e}{10^{16}}(r\nu)^{10} \quad (3)$$

The 12th order polynomial function is expressed as

$$f(x,y) = 1 + \frac{a}{10^3}(r\nu)^2 + \frac{b}{10^7}(r\nu)^4 + \frac{c}{10^{10}}(r\nu)^6 + \frac{d}{10^{13}}(r\nu)^8 + \frac{e}{10^{16}}(r\nu)^{10} + + \frac{f}{10^{19}}(r\nu)^{12} \quad (4)$$

where,

$$r = \sqrt{x^2 + y^2}.$$

Here r is the separation from the pointing position in arcmin, ν is the frequency in GHz, a, b, c, d, e and f are the coefficients of the polynomials.

Figs. 4 and 5 show the median (MED) RRLL beams and the average (AVG) RRLL beams for at the centre frequency 420 MHz of the 300–500 MHz data. These two Figures also show the corresponding

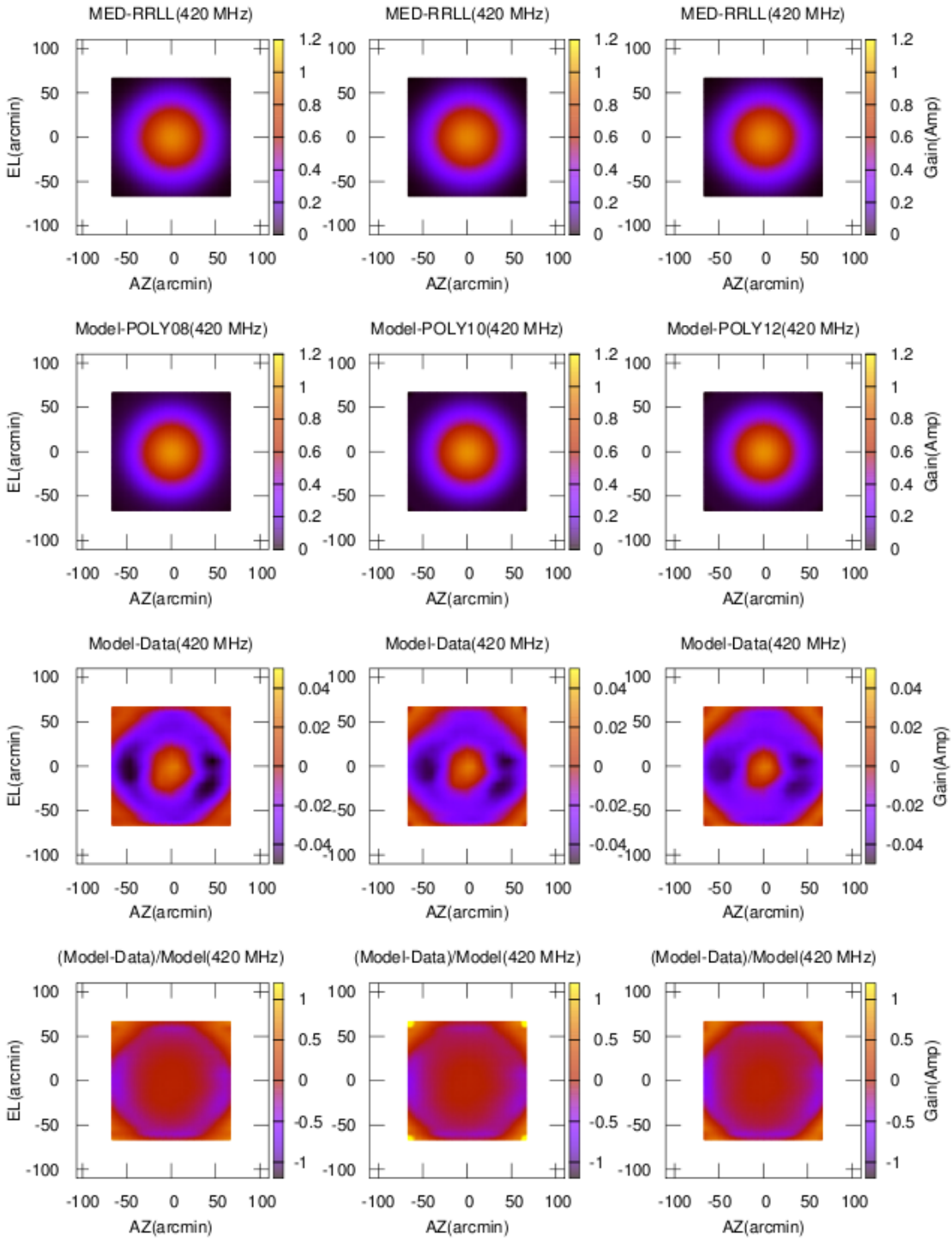

Figure 4: Figure showing the median (MED) RRLL beams at the centre frequency 420 MHz of the 300–500 MHz data. It also shows the corresponding model beams (second row panel), the difference between the data and the model beams (third row panel, and this difference divided by the model (fourth row panel). The three columns correspond to 8th order polynomial, 10th order polynomial and 12th order polynomial fits to the data.

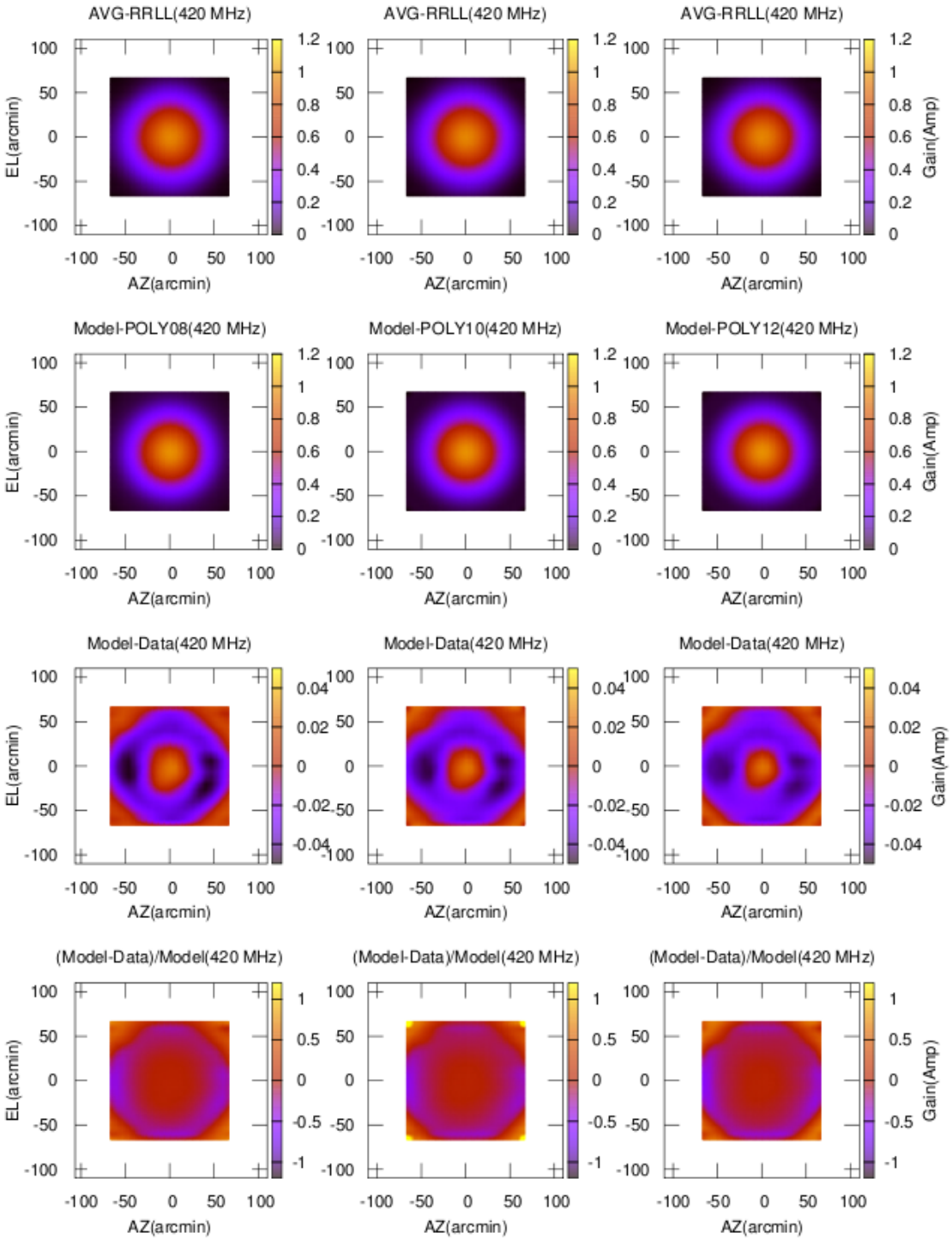

Figure 5: Figure showing the average (AVG) RRLL beams at the centre frequency 420 MHz of the 300–500 MHz data. It also shows the corresponding model beams (second row panel), the difference between the data and the model beams (third row panel, and this difference divided by the model (fourth row panel). The three columns correspond to 8th order polynomial, 10th order polynomial and 12th order polynomial fits to the data.

Table 2: Table showing RMS', data minus model (HPBW) for both, the surface and ring shapes shown in Fig. 7 of the 8th order polynomial, 10th order polynomial and 12th order polynomial fits for the (MED) RRLL beams. See also Sec. 4.4 for a detailed discussion and Fig. 8 for comparisons between 8th order polynomial, 10th order polynomial and 12th order polynomial fits.

RMS values, "data minus model" for 8th order, 10th order and 12th order polynomial fits							
Surfaces	RMS			Rings	RMS		
	$8^{\rm th}$	$10^{\rm th}$	$12^{\rm th}$		$8^{\rm th}$	$10^{\rm th}$	$12^{\rm th}$
25%	0.0298	0.0291	0.0284	0–25%	0.0298	0.0291	0.0284
50%	0.0244	0.0221	0.0201	25–50%	0.0225	0.0196	0.0170
75%	0.0194	0.0164	0.0148	50–75%	0.0142	0.0101	0.0092
100%	0.0158	0.0154	0.0148	75–100%	0.0101	0.0109	0.0127
125%	0.0158	0.0157	0.0154	100–125%	0.0143	0.0162	0.0155
150%	0.0164	0.0157	0.0146	125–150%	0.0189	0.0167	0.0141
175%	0.0159	0.0151	0.0140	150–175%	0.0168	0.0131	0.0125
200%	0.0159	0.0146	0.0140	175–200%	0.0123	0.0114	0.0119

model beam (second row), the difference between the data and the model beams (third row), and this difference divided by the model beams (fourth row). Note that in these two figures (Figs. 4 and 5), we provide these model fits for the 8th order polynomial (left column), 10th order polynomial (middle column) and 12th order polynomial (right column) fits for a faithful comparisons.

We also present the polynomial coefficients as a function of frequency for the three polynomials of 8th order (top-left panel), 10th order (top-right panel) and 12th order (bottom-left panel), respectively for the median (MED) RRLL (= Stokes I) beams in the three panels of Fig. 6. The coefficients themselves are also listed in Table 1.

4.4 Accuracy of the parametrization

In order to get an estimate of the expected accuracy of the primary beam correction, (i) the RMS value of the difference between the median beam and the model beam, and (ii) the maximum ("MAX") value of the (absolute) difference between the median beam and the model beam were also computed over both rings and annulus centered at the peak of the median beam. Fig. 7 show the rings and surface shapes used for this analysis. The sizes for the rings and annulus scale with the HPBW (e.g. if HPBW = 64 arcmin, then 50% =32 arcmin, 100% = 64 arcmin, and 200% = 128 arcmin). The RMS and MAX values are computed for both, (i) the difference between the median data and the polynomial model values at all pixel locations, and (ii) this difference (= median-data minus the polynomial-model values) normalized by the polynomial-model values at all pixel locations.

The two panels of Fig. 8 show the comparisons between the 8th order, 10th order and 12th order polynomial fits for the 0–200% surface data for (i) the RMS value of the difference between the median beam and the model beam (left-panel), and (ii) the maximum ("MAX") value of the (absolute) difference between the median beam and the model beam (right-panel).

These RMS values for the 8th order polynomial, 10th order polynomial and 12th order polynomial fits are tabulated (see Table 2) for different rings and surfaces shapes. The corresponding plots are presented in Figs. 9, 10 and 11. These Figures (Figs. 9, 10 and 11) and the table (Table 2) should provide users an indication of the expected error on the primary beam correction to the flux density. Furthermore, note that for both, rings and surfaces shapes, the RMS' are $\lesssim 5\%$ for 8th order polynomial, 10th order polynomial and 12th order polynomial fits. This suggests that higher order polynomial fits provide very little additional value, instead the 8th order polynomial is sufficient to provide meaningful science results.

These RMS values for the 8th order polynomial, 10th order polynomial and 12th order polynomial

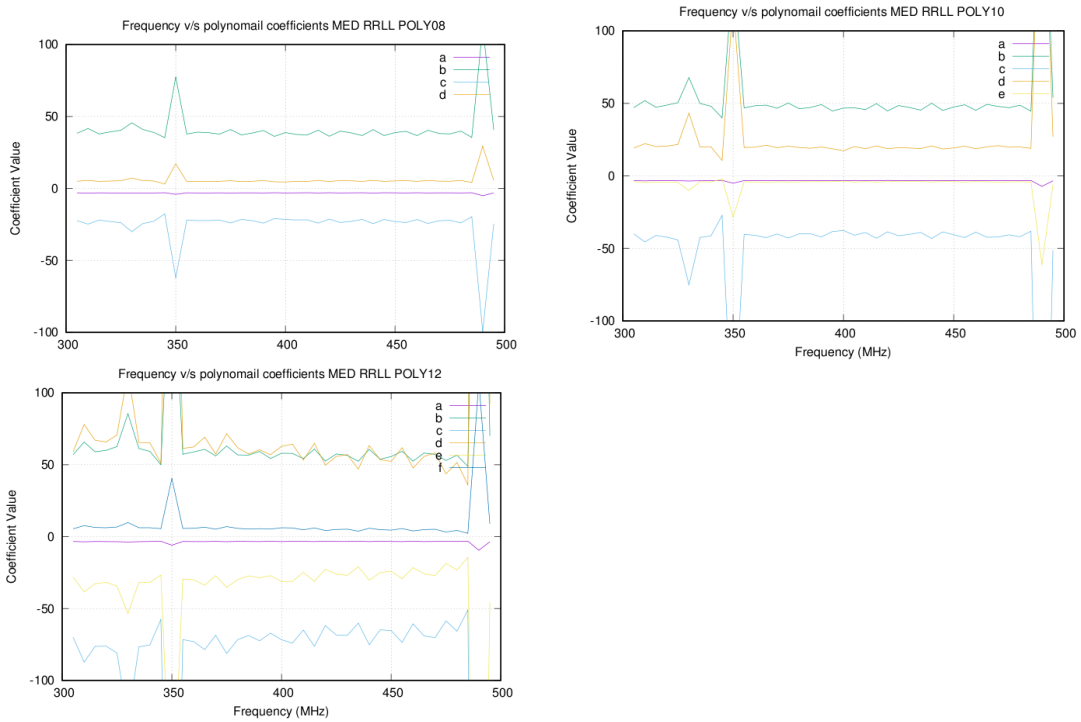

Figure 6: Figure showing polynomial coefficients as a function of frequency for the three polynomials of 8th order (top-left panel), 10th order (top-right panel) and 12th order (bottom-left panel) respectively for the median (MED) RRLL (= Stokes I) beams. The coefficients themselves are also listed in Table 1.

fits are tabulated (see Table 2) for different rings and surfaces shapes. The corresponding plots are presented in Figs. 9, 10 and 11. These Figures (Figs. 9, 10 and 11) and the table (Table 2) should provide users an indication of the expected error on the primary beam correction to the flux density. Furthermore, note that for both, rings and surfaces shapes, the RMS' are $\lesssim 5\%$ for 8th order polynomial, 10th order polynomial and 12th order polynomial fits. This suggests that higher order polynomial fits provide very little additional value, instead the 8th order polynomial is sufficient to provide meaningful science results.

4.5 Comparisons within antennas and with old polynomial coefficients

We now discuss the beam widths of all GMRT antennas for the azimuth and elevation axes, and we show both the median and mean beam widths. Note that we determine the median and the mean of the data sets for five epochs, we thus have azimuth and elevation beams for RRLL (= Stokes I) at all frequency-channels (spaced 5 MHz apart) of the 300–500 MHz band for all antennas. The 1σ errorbars shown in the mean beam widths is computed from the data sets for five epochs.

The estimated

$$\mathrm{HPBW} = 1.22 \times \frac{\lambda}{d} \tag{5}$$

suggests that the HPBW at 420 MHz for the 45 m parabolic dish $\simeq$ 66.6 arcminutes. Thus, in Fig. 12, we show the beam widths of all GMRT antennas at 420 MHz with good data; where the upper panel shows the mean beam width of all data and bottom panel shows the median beam widths of all data. We plot both, the beams along azimuth axis (red triangles) and along elevation axis (blue triangles) for antennas of GMRT. The green dotted line in it is the HPBW ($\simeq$ 66.6 arcminutes) at 420 MHz for the 45 m parabolic dish.

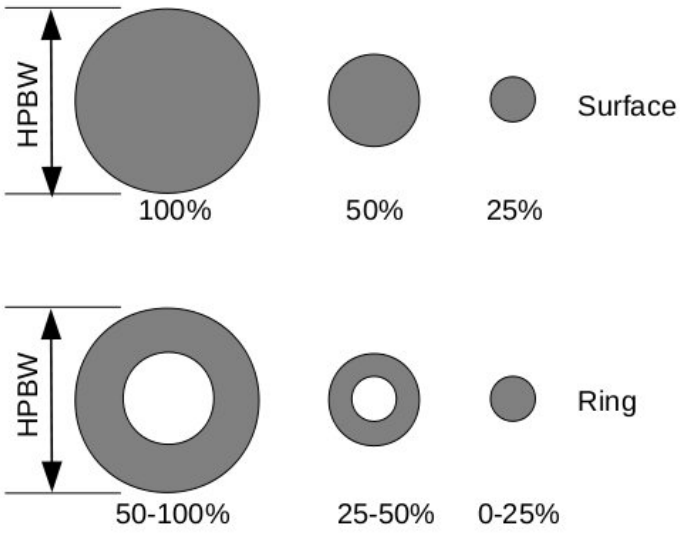

Figure 7: Figure showing the rings and surface shapes used to understand the expected accuracy of the primary beam correction. The sizes for the rings and annuli scale with the HPBW (for e.g., if HPBW = 64 arcmin, then 50% =32 arcmin, 100% = 64 arcmin, and 200% = 128 arcmin). See also Table 2 showing RMS' for both, the surface and ring shapes of the 8th order polynomial, 10th order polynomial and 12th order polynomial fits.

Next, we discuss the quality of five data sets. For C02 and E04 antennas, two data were bad, showed high and low beam widths, respectively, and hence it affected the mean beam widths for both, azimuth and elevation axes, and are not plotted. Similarly, for C03 and E06 antennas, three data sets were bad and they showed relatively small beam widths (with a small spread) and large beam widths (with a large spread) respectively. Hence, in the mean of C03 is relatively small and mean of E06 was too large, and beam widths for E06 are not plotted. Barring these outliers, i.e., antennas C02, C03, E04 and E06, the HPBW of all antennas are reasonable and has a mean (= 68.2 arcminutes) within 1-σ (= 1.8 arcminutes) errorbar. This mean of all antennas for both, azimuth and elevation axes is slightly larger than the HPBW (but consistent within errorbars) for the 45 m parabolic dish $\simeq$ 66.6 arcminutes at 420 MHz. Note that the mean and standard deviation are determined for the beam widths (FWHM) for the two, azimuth and elevation axes for all antennas presented in in Fig. 12.

Fig. 13 shows the comparisons between the old polynomial coefficients (in blue, from our earlier ver. 1 document, dated 2018-12-01), current (in red, recommended) 8th order polynomial coefficients, and the difference between the new (updated) and old polynomial coefficients (in green) at 420 MHz. The plot shows that the comparison between the earlier old polynomial coefficients and current 8th order polynomial coefficients too is consistent (Fig. 13), and the differences between the two HPBWs are less than 5% obtained for the two, old and new coefficients.

5 Summary of Results

We hope that this document, in particular Table 1 would be useful for the users of the GMRT in order to perform appropriate system checks, thereby improve the performance of the GMRT images at band-3.

In Figs. 4 and 5, we provide comparisons of the median and average RRLL beams at the centre frequency 420 MHz of the 300–500 MHz data. They also present the corresponding model beams, the difference between the data and the model beams, and this difference divided by the model for the 8th order polynomial, 10th order polynomial and 12th order polynomial fits to the data.

– Clearly there are no appreciable differences that are shown in the 10th order polynomial or the 12th order polynomial fits as compared to the 8th order polynomial fit.

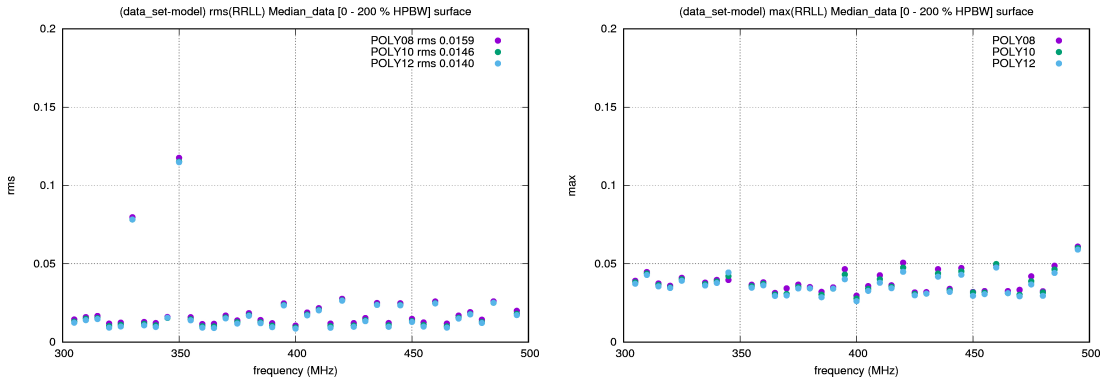

Figure 8: Plots showing the comparisons between the 8th order, 10th order and 12th order polynomial fits for the unnormalised data. Here, the two panels show the comparisons between the 8th order, 10th order and 12th order polynomial fits for the 0–200% surface data for (i) the RMS value of the difference between the median beam and the model beam (left-panel), and (ii) the maximum ("MAX") value of the (absolute) difference between the median beam and the model beam (right-panel).

– Furthermore, the accuracy of parametrization using the surfaces and rings (as detailed in Sec. 4.4) too do not reveal appreciable differences between the 10th order polynomial or the 12th order polynomial fits as compared to the 8th order polynomial fit (see also Table 1.

Although we provide a variety of Figures for users of the uGMRT to make a judgement re. the nature of polynomial fits, we believe that the 8th order polynomial is sufficient to draft science conclusions for the band-3, 250–500 MHz band of the uGMRT.

6 References

– Gupta, Y., et al. 2017 Cu. Sci. 113, 707

– Katore, S. N. & Chengalur, J. N. 2-D primary beam shape measurements of the band-5, 1050–1450 MHz of the uGMRT

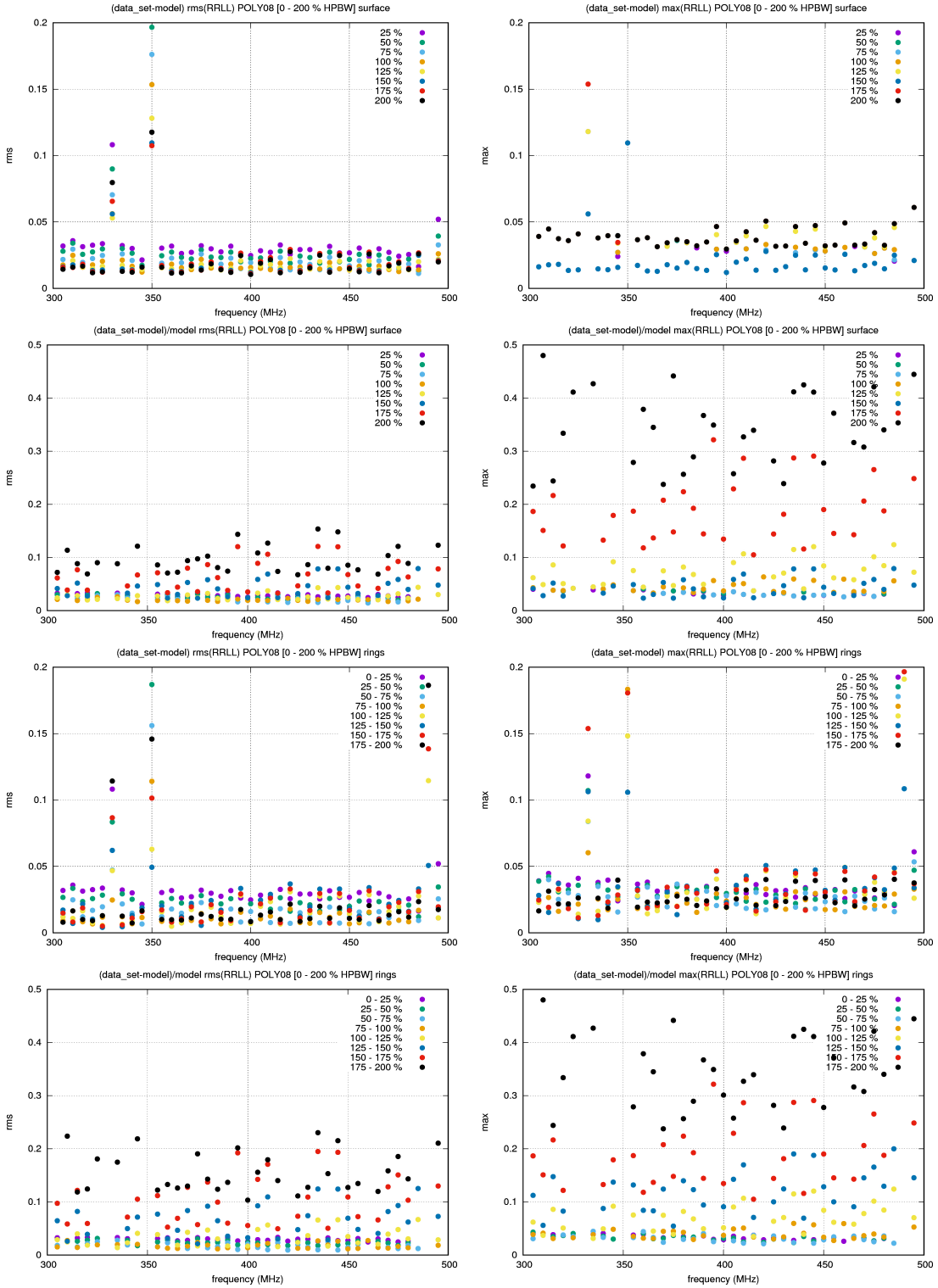

Figure 9: Plots showing the comparison between various surfaces and rings for the RMS values (left column panels) and the MAX values (right column panels) of the 8th order polynomial fits. The first and third row panels show the unnormalised (data minus model) polynomial fits and the third and fourth row panels show the normalised (data minus model divided by the model) polynomial fits.

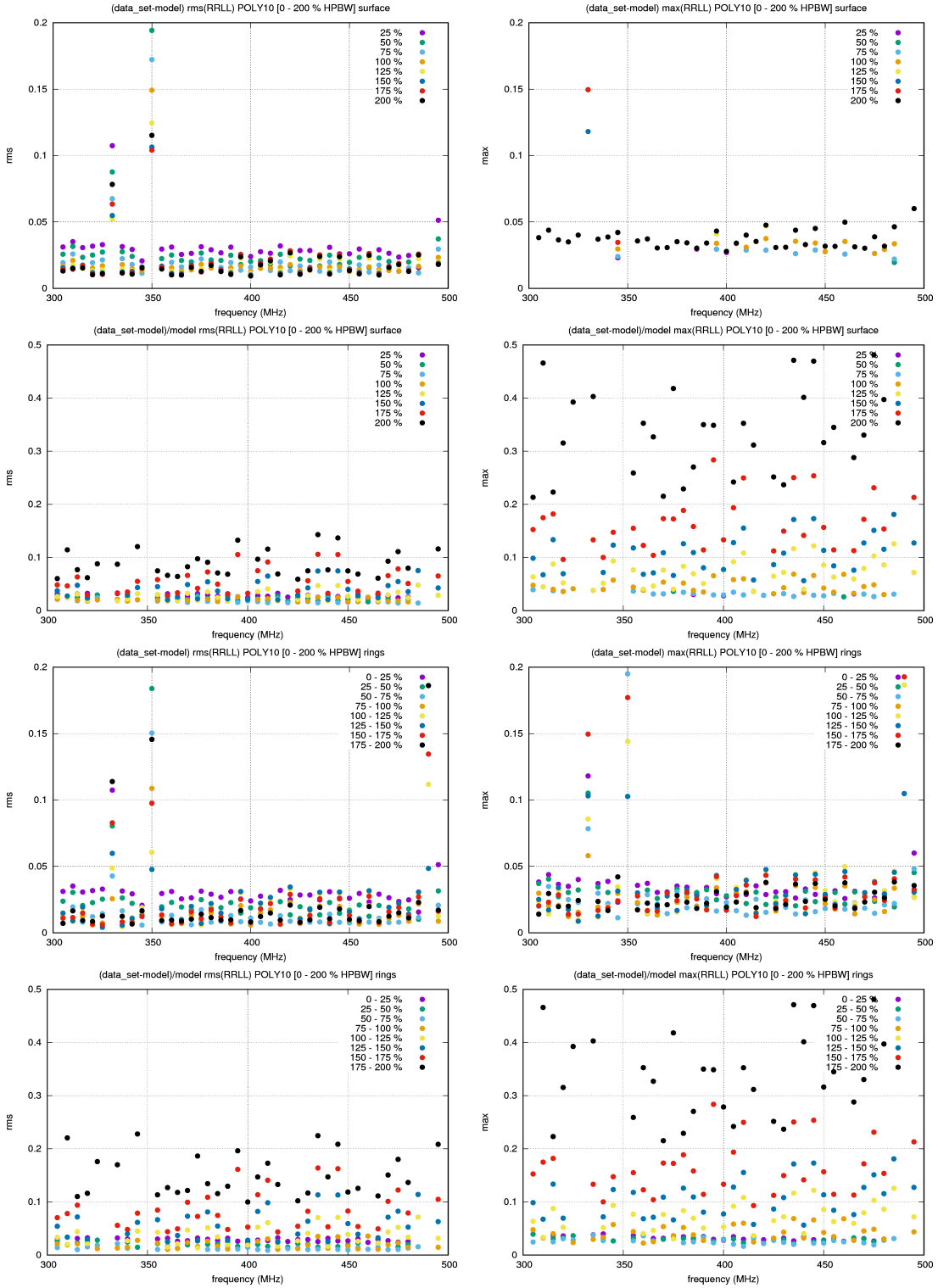

Figure 10: Plots showing the comparison between various surfaces and rings for the RMS values (left column panels) and the MAX values (right column panels) of the 10th order polynomial fits. The first and third row panels show the unnormalised (data minus model) polynomial fits and the third and fourth row panels show the normalised (data minus model divided by the model) polynomial fits.

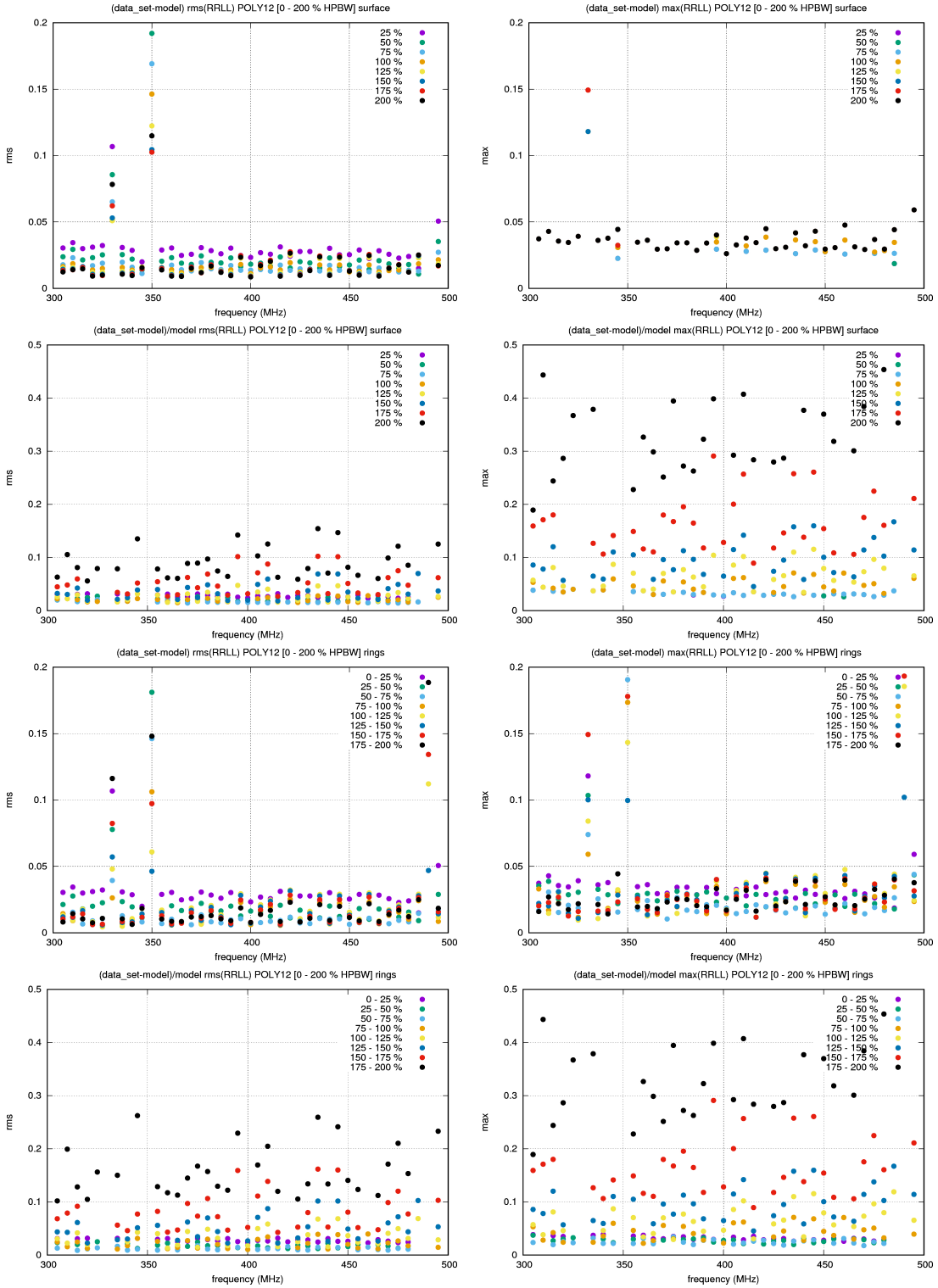

Figure 11: Plots showing the comparison between various surfaces and rings for the RMS values (left column panels) and the MAX values (right column panels) of the 12th order polynomial fits. The first and third row panels show the unnormalised (data minus model) polynomial fits and the third and fourth row panels show the normalised (data minus model divided by the model) polynomial fits.

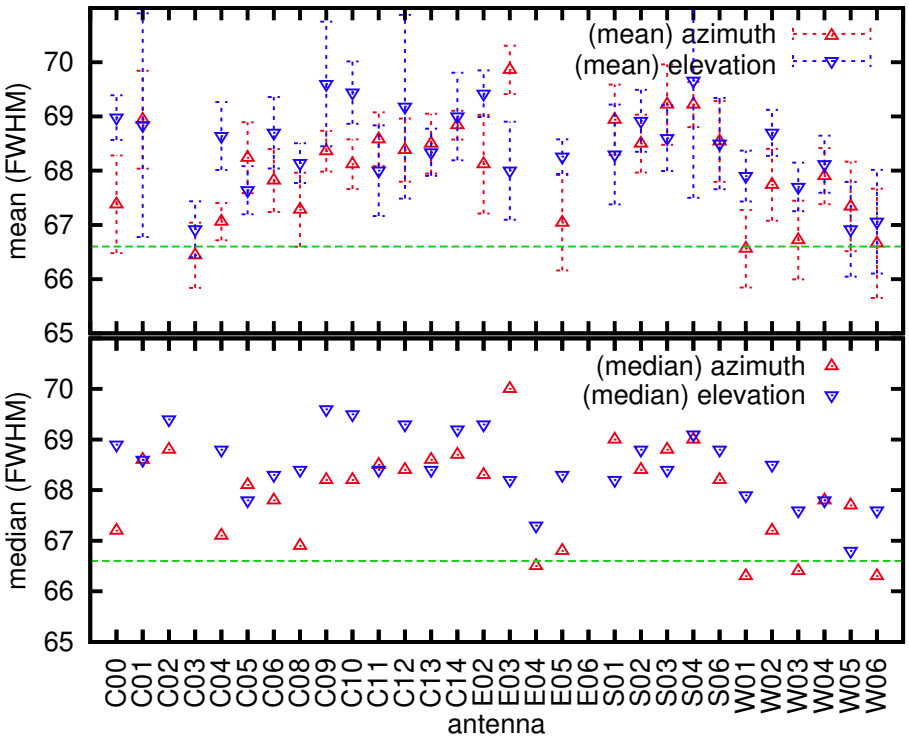

Figure 12: Figure showing beam widths of all GMRT antennas at 420 MHz with good data; where the upper panel shows the mean beam width of all data and bottom panel shows the median beam widths of all data. Here we plot both, the beams along azimuth axis (red triangles) and along elevation axis (blue triangle; see also Sec. 4.5 for a discussion). The green dotted line is the HPBW ($\simeq$ 66.6 arcminutes) at 420 MHz for a 45 m parabolic dish.

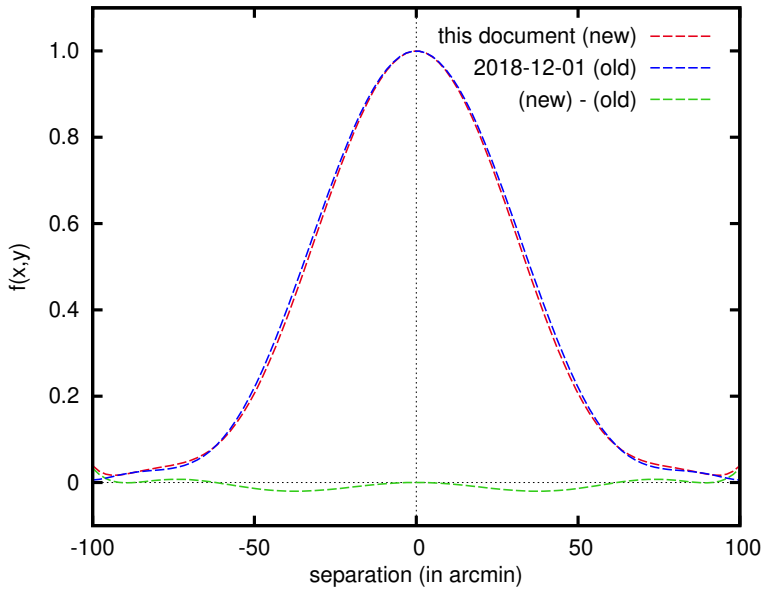

Figure 13: The comparisons between the old polynomial coefficients (in blue, from our earlier ver. 1 document, dated 2018-12-01), current (in red, recommended in this document) 8th order polynomial coefficients, and the difference between the new and old polynomial coefficients at 420 MHz (see also Sec. 4.5).